International Journal of Science and Research (IJSR)
ISSN (Online): 2319-7064
Index Copernicus Value (2015): 78.96 | Impact Factor (2015): 6.391

The use of Aeromagnetic Data Interpretation to Characterize the Features in the Mamfe Sedimentary Basin Cameroon and a Part of the East of Nigeria

Alain Rodrigue Nzeuga[1], Robert Nouayou[2], Françoise Enyegue à Nyam[3], James Derek Fairhead[4]

[1]Department of Physics, Faculty of Science, University of Yaounde I, P.O. Box 812, Yaounde, Cameroon

[2]Department of Physics, Faculty of Science, University of Yaounde I, P.O. Box 812, Yaounde, Cameroon

[3]Department of Physics, Faculty of Science, University of Yaounde I, P.O. Box 812, Yaounde, Cameroon

[4]School of Earth and Environment, Faculty of Environment, University of Leeds, UK

Abstract: ***The aeromagnetic data of the Mamfe Sedimentary Basin (MSB) and a part of the East of Nigeria was used to carry out the main features of that study area. To achieve this goal, we have used firstly, the horizontal gradient of the total magnetic intensity field reduced to the pole and the analytical signal of the total magnetic intensity field for the determination of the magnitude maxima of them, and finally the contacts directions deducted by Euler's solutions. The suggested structural map of the study area presents the fault system of the zone, and the positions of the intrusions of the igneous bodies that can help in an orientation for a geophysical investigation. It also justifies the complexity of the tectonics of the region and reveals geological structures that the previous methods could not identify.***

Keywords: Aeromagnetic, Horizontal gradient, Analytic signal, Lineament, Fault.

1. Introduction

The MSB was borned from the opening of the south Atlantic during the Cretaceous followed by the accumulation of marine sediments in the Benue trough during the Albian [1], [2]. It is the smallest of the three side rifts associated with the Benue trough and it extends from the lower Benue trough in Nigeria into southwestern Cameroon where it narrows and terminates under the Cameroon Volcanic Line [3].

In this area, many geological and geophysical studies have been carried out. Geological studies include the works of Le Fur [4], Dumort [5], Njonfang [6], Hell et al. [7], Eseme [8], Eyong [9], Sa'a [10] and geophysical works include the works of Collignon [11], Petters et al. [12], Fairhead and Binks [13], Poudjom Djomani et al. [14], Ndougsa Mbarga [3], Nouayou [15], Nguimbous-Kouoh et al. [16]. All of these geophysical studies were done using gravity, audio magnetotelluric and helio magnetotelluric data.

The aeromagnetic data has never been used in this area for geophysical studies. Contrary to the preceding geophysical studies used in the Mamfe sedimentary basin, aeromangetic method is a geophysical prospection method used in a large spectrum since it has as advantage the fact that it does not depend on vegetation density and access difficulty. The aim of this work is to use aeromagnetic data to characterize the shallow structures of the area of interest and propose a comprehensive structural map. To achieve this, various interpretation methods are used. First of all, a total magnetic intensity anomaly map of the area of interest is undertaken. Based on the filtering of the total magnetic intensity map reduced to pole and the total magnetic intensity anomaly map, we inferred the main features of the basin structure and next we had to compare this result with that obtained from the previous studies in the area.

2. Geology of the study area and tectonic setting

The MSB is a WNW-ESE trending trough that covers an approximately area of 2400 Km^2 and it is one of the non-intracratonic producer basin that exists in Cameroon (Figure 1 (a)). The area of interest is located between the latitudes 5° 30' N and 6° 00' N, and longitudes 8° 50' E and 9° 50' N (Figure 1 (b)). It is a plane surface that underwent a light rise [5] with average altitude ranging between 90 m and 300 m above sea level [16]. The mark of many minerals like sapphire, lignite, zinc and lead and important oil fields were discovered in the basin [5, 7, 9, 15, 17, 18, 19, 20, 21].

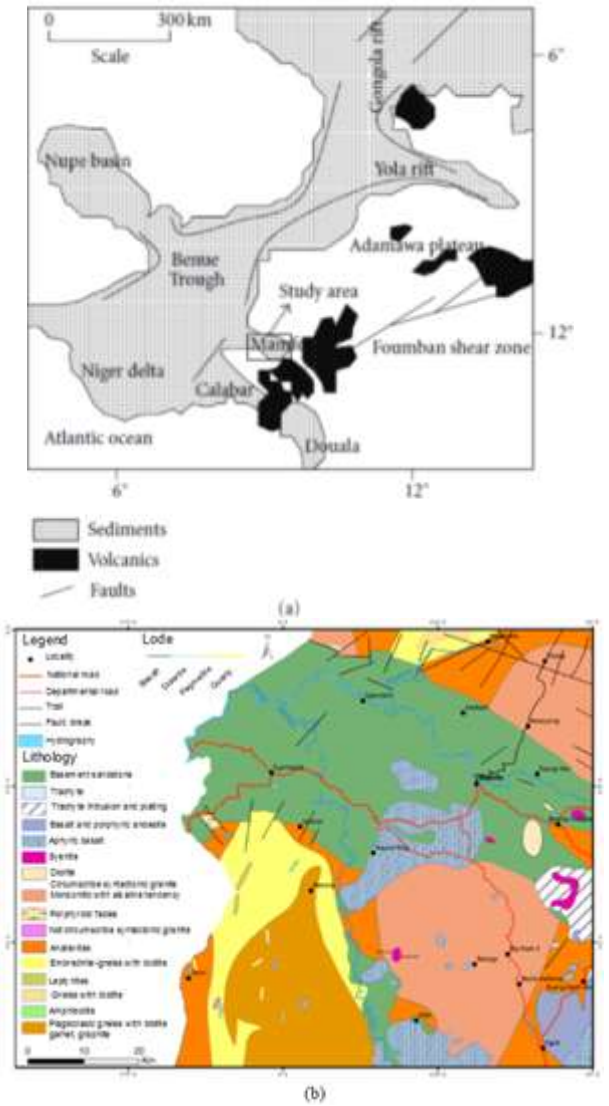

Figure 1: Geological map of the study area. (a): Map showing the location of the study area and the location of rifts in the Benue Trough [18]. (b): Geological map of the Mamfe basin [5].

The MSB is made of horst and grabens. The major tectonic activity is described by two main phases known as an extension phase and a compression phase. The extension phase is characterized by the formation of many faults in the basin some of which were observed on the Manyu [15], and the compression phase is characterized through the anticline and syncline pattern of the basin, and a late formation of some faults and break [5, 9].

The geological features of the basin belong to all great groups of rocks we know. We can distinguish the following formations: basement, sediments, magmatic and post-cretaceous metamorphic.

According to Le Fur [4], five series of sedimentary rocks are recognized in the eastern part of the Mamfe basin (Figure 2). From top to bottom [21] they include:
a) Cross River sandstone series,
b) Clayey sandstone series,
c) Upper conglomeratic sandstone series,
d) Manyu sandy clay series,
e) Lower conglomeratic sandstone series.

Lithology	Description	Age
	Basalts, syenites, and trachytes	Tertiary
	Sandstones, arkosik, and conglomeratic	Cenomanian
	Oolitic, shales with centimetric veinlets of lignite, and bituminous shales	Albian
	Conglomerates overlain by arkosic sandstones showing cross bedding	
	Siliceous and calcareous shales intercalated with arkosic sandstones	
	Conglomeratic sandstones with arkosic cements containing basement fragments up to 15 cm in diameter	
	Basement made up of granites schists and gneisses	Precambrian

Figure 2: Generalized stratigraphic column of the Mamfe Basin showing ages of units, lithology and probable source rocks [4, 21].

3. Data acquisition and processing

3.1 Aeromagnetic data

The data used in the study are from the compilation of two aeromagnetic surveys acquired by SURVAIR (contractor) company in Cameroon for CIDA (client) in 1970 and POLSERVICE-GEOPOL (contractor) in Nigeria for MINES AND POWER (client) in 1976. In Cameroon, aeromagnetic surveys were done with a flight height of 235 m and a line spacing of 1000 m and in a direction line of 0, and the one for Nigeria was flown with a flight height of 150 m, a line spacing of 2000 m and in a direction line of 150. After applying the IGRF filter we noted that the data had already been processed and values of the magnetic field provided were those of the total magnetic intensity anomaly (TMI).

3.2 Data processing

Several interpretation methods were applied for the purpose of bringing out the lineament and the traces of hidden faults. These methods included reduction of total magnetic intensity to pole, upward continuation, horizontal gradient and analytic signal.

3.2.1 Total Magnetic Intensity method (TMI)

The data was gridded with a cell size of 500 m grid space to show the spatial distribution of magnetic anomaly. The amplitude of magnetic anomaly is directly proportional to magnetization which depends on magnetic susceptibility of the rocks [22]. The TMI map showed the differences in locations of high and low magnetic intensities (Figure 3). Also, differences in locations of high and low magnetic intensities and many crustal magnetization patterns were illustrated.

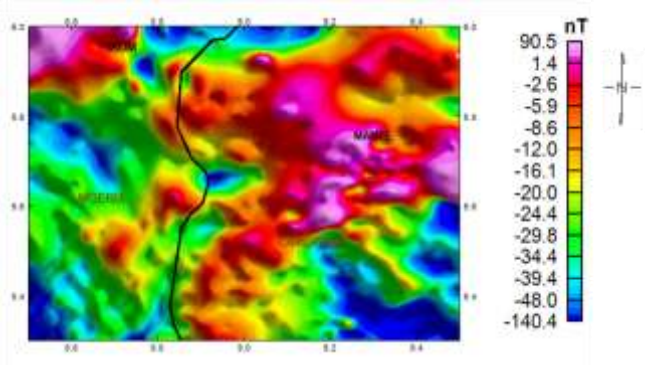

Figure 3: Total magnetic intensity map of the study area.

3.2.2 Reduction to the Pole method (RTP)

Close to the earth's equator low susceptible magnetic features appeared as high magnetic anomalies and vice versa [22]. To remove the influence of magnetic latitude on the residual anomalies [23], a reduction to the pole (RTP) filter was applied to the TMI grid in order to locate the observed magnetic anomalies directly over the magnetic source bodies that caused the anomaly. The TMI grid was transformed into reduction to the pole grid using the 2D-FFT (Fast Fourier Transform) filter in Geosoft Oasis Montaj software V 6.3. The parameters taken on the 01/01/1970 according to IGRF were at an inclination of - 11.968° and declination of - 6.270° which represented the mean value for the area.

The RTP magnetic anomaly map (Figure 4) shows both low and high magnetic frequencies representing points of low and high magnetic signatures respectively in the area.

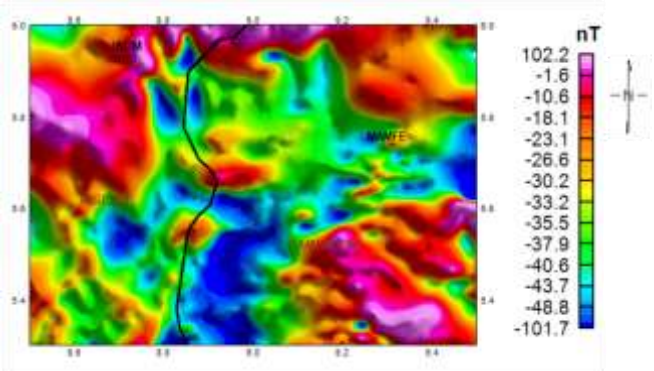

Figure 4: Total magnetic intensity map reduced to the pole.

3.2.3 Upward Continuation method

Figure 5 (a-b) shows the TMI upward continued grid up to 2000 m and 3000 m respectively; i.e., they showed images of the magnetic intensity that were obtained assuming the data was recorded at heights of 2000 m and 3000 m, higher than the original collected datum data. These grids were processed to calculate and display the corresponding analytic signal grids and get their grid peaks locations. Figures 5 (c-d) also shows the RTP upward continued grid up to 2000 m and 3000 m respectively and from TMI these grids were processed to calculate and display the corresponding horizontal gradient grids to get their peak locations.

In physical terms, as the continuation distance increased, the effects of smaller, narrower and thinner magnetic bodies progressively disappeared relative to the effects of larger magnetic bodies of considerable depth extent. As a result, upward-continuation maps gave the indications of the main tectonic and crustal blocks in the area.

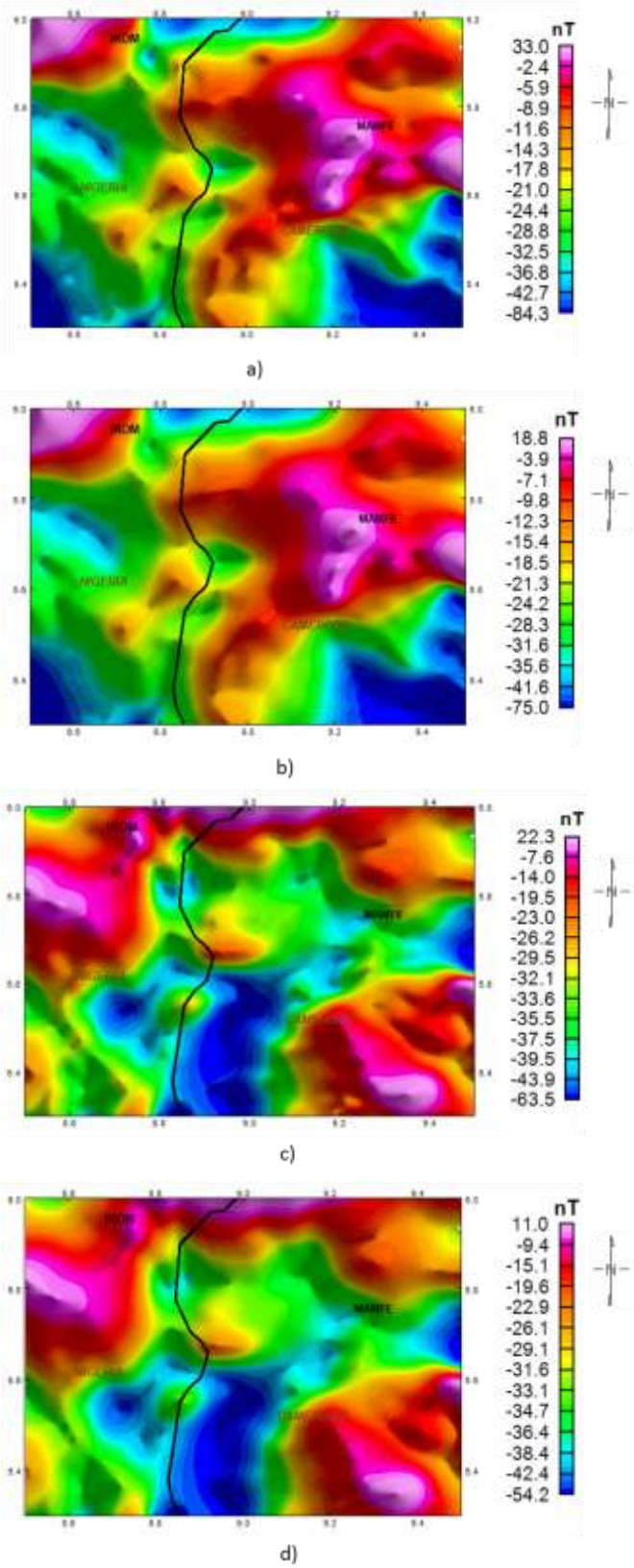

Figure 5: (a-b) TMI upward continued grid up to 2000 m and 3000 m respectively; (c-d) RTP upward continued grid up to 2000 m and 3000 m respectively.

3.2.4 Horizontal Gradient method

The horizontal gradient method is one of many approaches used to estimate contact locations of a body at depths. Its biggest advantage is its low sensitivity to noise in the data because it only requires calculations of the two first-order horizontal derivatives of the field [24]. In the spatial domain, the horizontal gradient or horizontal derivative (HD) of the total magnetic field T is given by:

$$HD(x, y) = \sqrt{\left(\frac{\partial T}{\partial x}\right)^2 + \left(\frac{\partial T}{\partial y}\right)^2} \quad (1)$$

According to Phillips [24], this function gives a peak anomaly above magnetic contacts under the following assumptions: (1) the regional magnetic field is vertical, (2) the magnetizations are vertical, (3) the contacts are vertical and isolated, (4) the sources are thick.

Transgression of the first three assumptions can lead to a translation of the peaks away from the contacts. Transgression of the fourth assumption can lead to secondary peaks parallel to the contacts. Thus in low latitude, the existence of horizontal gradient corresponds to a presence of a magnetic susceptibility contrast. We apply the horizontal gradient directly on a map of total magnetic intensity reduced to the pole rather than the TMI map. The reduction of the field to the pole made the regional magnetic field to be horizontal and most of the source magnetizations to be horizontal.

Figures 6 (a) and 6 (b) shows the horizontal gradient of TMI-RTP upward to 2000 m and 3000 m respectively which will be used to determine the corresponding maxima of the horizontal gradient.

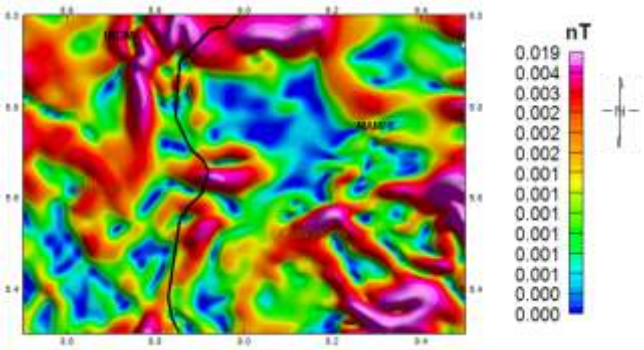

Figure 6(a): Horizontal gradient of TMI-RTP upward to 2000 m.

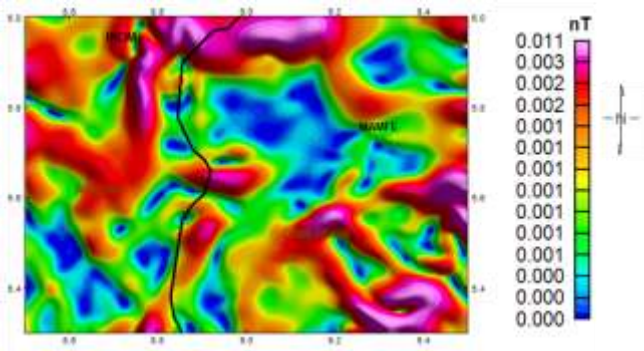

Figure 6(b): Horizontal gradient of TMI-RTP upward to 3000 m.

3.2.5 Analytic Signal method

To know the source positions of the magnetic anomaly regardless of direction and remanent magnetization in the sources effect that is mostly associated with the RTE, the analytic signal filter was applied to the TMI grid. The significant characteristic of the analytic signal is that, it is independent of the direction of magnetization of the source [25], [26]. Moreover, the amplitude of the analytic signal can be related to the amplitude of magnetization [27], [28]. The amplitude of the analytic signal of the anomaly T of the intensity of magnetic field is given by [25]:

$$AS = \sqrt{\left(\frac{\partial T}{\partial x}\right)^2 + \left(\frac{\partial T}{\partial y}\right)^2 + \left(\frac{\partial T}{\partial z}\right)^2} \quad (2)$$

Figure 7(a) and 7(b) shows the analytic signal of TMI upward to 2000 m and 3000 m respectively which will be used to determine the corresponding maxima of the analytic signal.

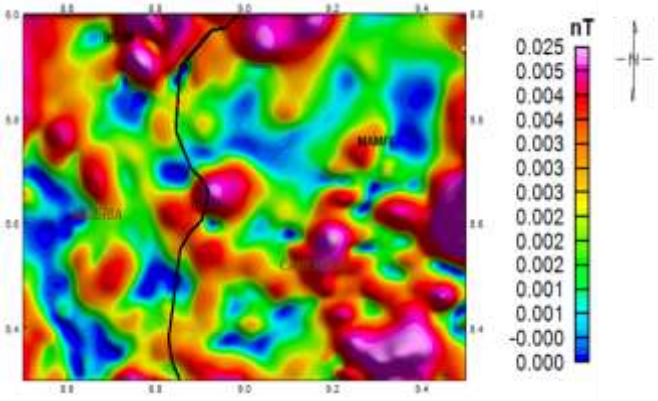

Figure 7(a): Analytical Signal of TMI upward to 2000 m.

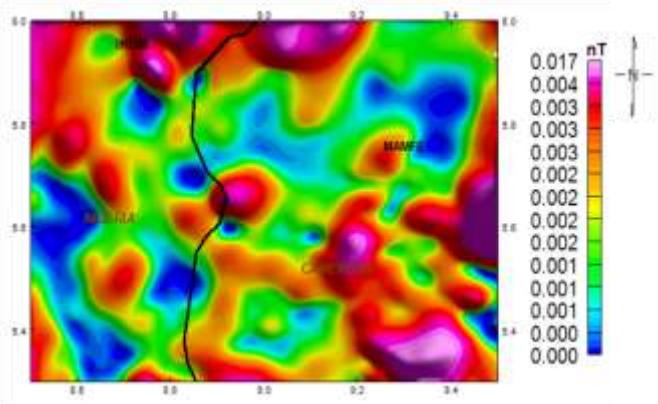

Figure 7(b): Analytic Signal of TMI upward to 3000 m.

4. Data interpretation and results

To determine deep faults located between 2 and 3 km in the MSB, we first determine the maxima of the maps of Horizontal gradient of TMI-RTP upward to 2000 m and 3000 m, then, the maxima of the maps of Analytic Signal of TMI upward to 2000 and 3000 m all by the method of Blakely and Simpson [29]. Finally, we will combine all the four maps to determine the structural map of the MSB and to validate our results, we will compare the obtained structural map with the Euler deconvolution map of the study area.

4.1 Results of analyzing horizontal gradient maps

The horizontal gradient maps represented on figures 6 (a) and 6 (b) shows in general major anomalies in WSW-ENE direction with amplitudes of gradient reaching 0.02 nT. The highly positive anomalies observed on the map have circular shapes and could represent the signature of intrusive bodies. In the South and in the South-east part of the MSB, the zones of high gradients appear in various forms and justify the complexity of the tectonics of the MSB. The maxima of the maps of upward horizontal gradient up to 2 and 3 km were plotted to highlight the contacts direction on them (Figure 8).

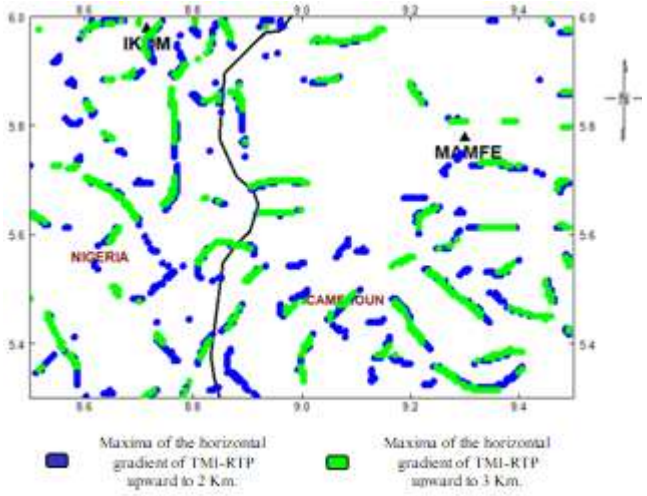

Figure 8: Maxima of the horizontal gradient magnitude of the TMI-RTP upward to 2 and 3 km.

This map reveals structural complexity of the study area. The lineaments located here show linear contacts that can correspond to faults, circular contacts that can correspond to the horizontal contours of intrusive body boundaries and magnetic strips that can be assimilated to domes or folds.

4.2 Results of the analysis of the maps of analytic signal

On the maps of Analytic Signal of TMI upward to 2000 m and 3000 m represented on figure 7 (a and b), we can observe that there are analogies between these maps and those of the horizontal gradient magnitude upward to 2000 m and 3000 m respectively. The anomalies observed are of direction WSW-ENE and their gradients reach values of 0.025 nT. In general, the zones of positive anomalies observed on the map of Total magnetic intensity reduced to the pole and on the maps of horizontal gradient are well marked on the maps of analytic signal. All of these reinforce the hypothesis of the presence of intrusive bodies in these places with high magnetic susceptibility relative to that of the host formation.

To highlight the contacts direction shown on the maps of analytic signal, the maxima of the maps of analytic signal upward to 2 and 3 km were plotted on figure 9.

The lineaments located here show only linear contacts that can correspond to faults.

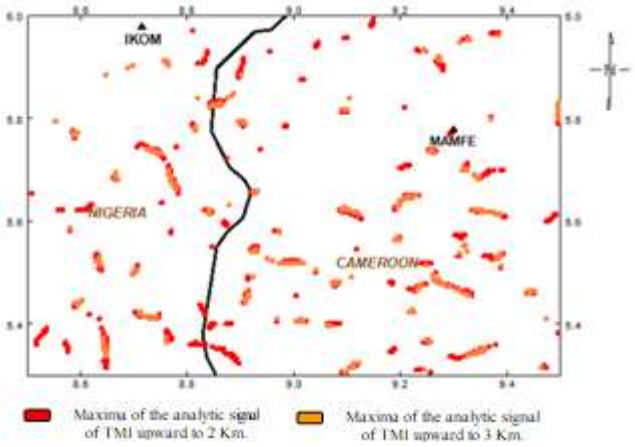

Figure 9: Maxima of the analytical signal of the TMI upward to 2 and 3 km.

4.3 Estimated location of contacts of the study area

To determine the geological contacts of the MSB, we proceed by the superposition of maxima graphs of the horizontal gradient (Figure 8) and that of the maxima for analytic signal (Figure 9) that we can see on figure 10. Also, the zones where the maxima joint represent geological contacts which will be interpreted at the end and their nature determined.

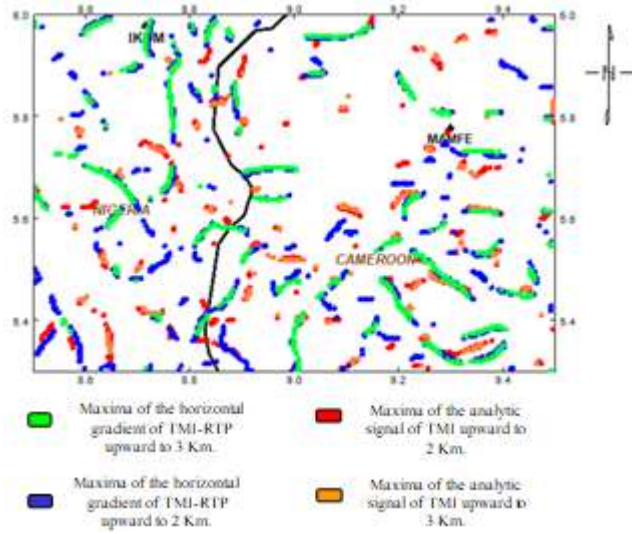

Figure 10: Map of superposition of the maxima of the horizontal gradient of the total magnetic intensity reduced to pole upward to 2 and 3 km and that of the maxima of the analytic signal of total magnetic intensity upward to 2 and 3 km.

4.4 Contribution of Euler's 3-D deconvolution

Euler's deconvolution was applied to the grid of magnetic anomalies with the following parameters: N = 1, Z = 15%, W = 10x10, H = 235 m with the aim of putting into evidence all the structures of the different contacts/faults, giving their directions and their mean depth. Figure 11 represents the graph of Euler's deconvolution on which we can notice that their contacts in most cases are of directions WSW-ENE and NO-SE, and this justifies also the results obtained from the graphs of horizontal gradient and analytic signal.

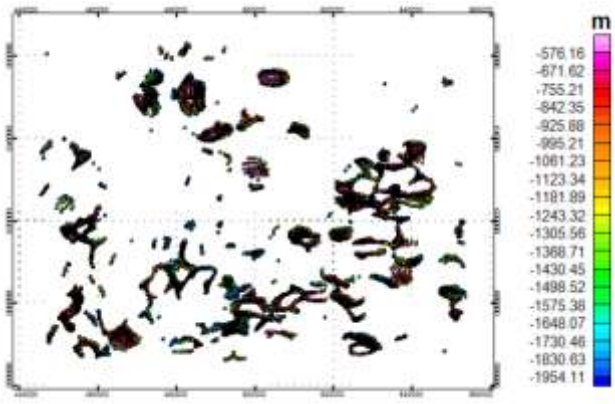

Figure 11: Euler's solution map of the study area.

4.5 Structural map of the study area and interpretation of features

The maxima observed on the figure 10 will be analyzed to determine the observed directions of geological contacts in the MSB. The represent contacts on figure 12 were drawn based successively on the results of the graphs of the maxima of horizontal gradient, maxima of analytic signal and the grid of Euler's deconvolution. The method used stipulates that when the maxima of the horizontal gradient and that of analytic signal are superimposed it gives fault and where contacts of horizontal gradient are parallel to analytic signal and slightly offset from them, the analytic contact represent the true feature location and the down dip direction is illustrated by the horizontal gradient contacts. Figure 13 represents rosace of the faulting direction plotted and table 1 the principal contact directions identified at different depths comprised between two and three kilometers which are interpreted as faults. Next, base of the Euler's deconvolution graph, we will justify the results represented on figure 13 and table1.

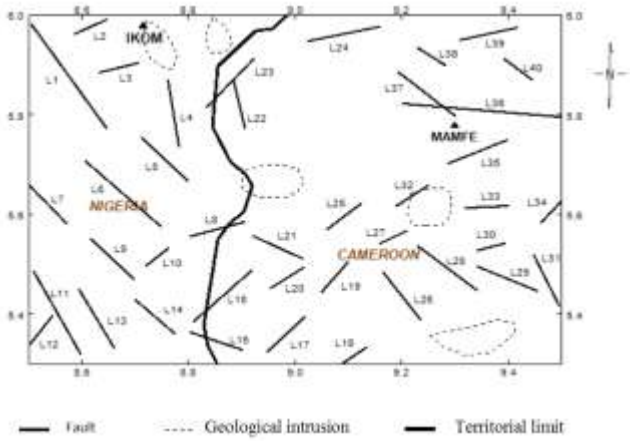

Figure 12: Structural map of the study area

The contacts underlined on this structural sketch are represented under two different natures:

- Faults (*in strong lines*), which can represent zones of main tension formed during the opening time of the South Atlantic;
- A geological intrusion (*in interrupted line*), which can be assimilated to an intrusion of igneous bodies into the sediments.

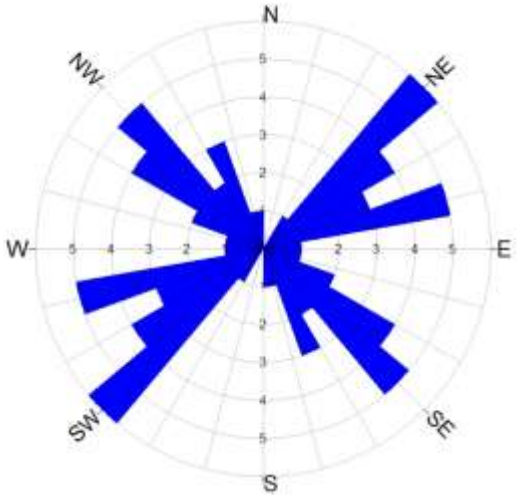

Figure 13: Rosace of faulting cartography.

Table 1: Directions of principles contacts interpreted as faults

Fault	*Direction*		*Fault*	*Direction*
L1	*N146°E*		*L21*	*N116°E*
L2	*N66°E*		*L22*	*N166°E*
L3	*N75°E*		*L23*	*N43°E*
L4	*N171°E*		*L24*	*N78°E*
L5	*N135°E*		*L25*	*N51°E*
L6	*N133°E*		*L26*	*N143°E*
L7	*N137°E*		*L27*	*N63°E*
L8	*N74°E*		*L28*	*N128°E*
L9	*N135°E*		*L29*	*N113°E*
L10	*N50°E*		*L30*	*N75°E*
L11	*N152°E*		*L31*	*N155°E*
L12	*N38°E*		*L32*	*N56°E*
L13	*N150°E*		*L33*	*N87°E*
L14	*N132°E*		*L34*	*N42°E*
L15	*N110°E*		*L35*	*N67°E*

L16	*N47°E*		*L36*	*N95°E*
L17	*N45°E*		*L37*	*N129°E*
L18	*N55°E*		*L38*	*N125°E*
L19	*N41°E*		*L39*	*N77°E*
L20	*N56°E*		*L40*	*N128°E*

Generally, we can notice that during the opening of the Atlantic south, two major fracture directions were noticed in the study area which are: NE-SW and NW-SE, and these results justify that obtained from Euler's deconvolution map.

5. Conclusion

Firstly, the use of aeromagnetic method for the characterization of MSB structures has permitted us to put into evidence several structures which were not identified by the previous geophysical methods used by different researchers in the area and also to show that the rocks within the basement principally have induced magnetism. The analysis of the maps of maxima of horizontal gradient of the total magnetic intensity reduced to the pole and the amplitude of the analytic signal of the total magnetic intensity has contributed to the putting in place of the faulting system responsible for the structuring of the MSB. The structural interpretative map justifies the structural directions observed from filtering maps and puts in place the frequency of directions N50°E to N75° E and N120°E to N150°E. This map also show the geological features found in the study area and all these information constitute important elements which can help as orientation for exploration and exploitation of natural resources in the study area.

Lastly, figure 13 above justifies the complexity of the tectonic nature of the region contrary to the results obtained by Collignon (1968) and the studies carried out in the area. This difference can be explained either (i) by the limit of geophysical methods used in the past at the level of data collection or by (ii) rapid evolution of the tectonic nature of the region with time.

6. Acknowledgements

The authors thank GETECH Group plc (Leeds, UK) for providing aeromagnetic data used, and the anonymous reviewers for their remarks that will enable us to improve this research work.

References

[1] M. C. Daly, J. Chorowicz, J. D. Fairhead, "Rift basin evolution in Africa: The influence of reactivated steep basement shear zones", In M. A. Cooper and G. D. Williams (editors). Inversion tectonics. Géol. Soc. Spec. Publ., pp 309-334, 1989.

[2] J. Benkhellil, "Structure et évolution géodynamique du bassin intracontinental de la Bénoué (Nigéria) ", Thèse de Doctorat, Univ. Nice, France, 295 pages, 1986.

[3] T. Ndougsa-Mbarga, "Etude géophysique par méthode gravimétrique dans les structures profondes et superficielles de la région de Mamfé", Thèse de Doctorat/PhD, Université de Yaoundé I, 255 pages, 2004.

[4] Y. Le Fur, "Mission socle-Crétacé. Rapport 1964-1965 sur les indices de plomb et de zinc du golfe de Mamfé", Tech. Rep., Rapport B.G.R.M., Cameroun, 1965.

[5] J. C. Dumort, "Notice explicative sur la feuille Douala-Ouest", Direction des Mines et de la Géologie du Cameroun, 69p, 1968.

[6] E. Njonfang, "UN exemple de complexe pluto-volcanique tertiaire à roches basiques et intermédiaires: le massif de Nda Ali, Sud-Ouest du Cameroun", Thèse de Doctorat 3ème cycle, Université de Yaoundé, Cameroun, 192p, 1986.

[7] J. V. Hell, V. Ngako, A. B. Béa, J. B. Olinga, J. T. Eyong, "Rapport des travaux sur l'Etude de Reconnaissance Géologique du bassin sédimentaire de Mamfé", I.R.G.M. – S.N.H., vol. 1, 20 p, 2000 (unpublished).

[8] E. Eseme, "Geochemistry of salt spring in the Southwestern Mamfe Basin and its significance to applied sedimentology", Master's in applied geology, University of Buea, Cameroon, 147 p, 2001.

[9] T. J. Eyong, "Litho-biostratigraphy of the Mamfe Cretaceous Basin, S. W. Province of Cameroon, West Africa", PhD Thesis University of Leeds, School of Earth Sciences, 256 pages, 2003.

[10] P. J. B. Sa'a, "Etude sédimentologique des faciès détritiques de la moitié Est du bassin de Mamfé : essai d'interprétation paléogéographique et intérêt pétrolier", Mémoire de Masters of Sciences, Université de Dschang, 126 pages, 2007.

[11] F. Collignon, Gravimétrie de reconnaissance de la République Fédérale du Cameroun, O.R.S.T.O.M., Paris, 35 p, 1968.

[12] S. W. Petters, C. S. Okereke, C. S. Nwajide, "Geology of the Mamfe rift, S.E. Nigeria", In Matheis G. and Schandelmeier eds., Current research in Africa Earth Sciences: Rotterdam, Balkema, pp. 229-302, 1987.

[13] J. D. Fairhhead, R. M. Binks, "Differential opening of the Central and South Atlantic Ocean and the opening of the West African rift system", Tectonophysics, 187, pp. 191-203, 1991.

[14] Y. H. Poudjom-Djomani, D. B. Boukeke, A. Legeley-Padovani, J. M. Nnange, Ateba-Bekoa, Y. Albouy, J. D. Fairhead, Levés gravimétriques de reconnaissance du Cameroun, ORSTOM, France, 30p, 1996.

[15] R. Nouayou, "Contribution à l'étude géophysique du bassin sédimentaire de Mamfé par prospections Audio et Hélio Magnétotelluriques", Thèse de Doctorat d'Etat ès Sciences, Université de Yaoundé I, 212 pages, 2005.

[16] J. J. Nguimbous-Kouoh, E. M. Takam Takougang, R. Nouayou, C. T Tabod, E. Manguellé-Dicoum, "Structural Interpretation of the Mamfe Sedimentary Basin of Southwestern Cameroon along the Manyu River using Audiomagnetotellurics Survey", International Scholarly Research Network Geophysics, volume 2012, 7 pages, 2012.

[17] M. M. Eben, Report of the Geological expedition in the Gulf of Mamfe: Archives of the Department of Mines & Geology, Ministry of Mines & Power, Cameroon, 10p, 1984.

[18] J. D. Fairhead, C. S. Okereke, J. M. Nnange, "Crustal structure of the Mamfe Basin, West Africa, based on gravity data", Tectonophysics, pp.351-358, 1991.
[19] R. Kangkolo, "Aeromagnetic study of the Mamfe basalts of southwestern Cameroon", Journal of the Cameroon Academy of Sciences, 2(3), 173-180, 2002.
[20] Ndougsa Mbarga, T. and Gweth Ntep, P., 2005. Report on the Mamfe salt and sapphire reconnaissance expedition. Internal Report Archives N°0058/2005 of the Ministry of Industry, Mines and Technological Development, 12 pp.
[21] E. Eseme, C. M. Agyingi, J. Foba-Tendo, "Geochemistry and genesis of brime emanations from Cretaceous strata of the Mamfe Basin, Cameroon", Journal of African Earth Science, vol. 35, n°4, pp. 467-476, 2002.
[22] P. J. Gunn, P. R. Miligan, "Enhancement and presentation of airbone geophysical data", AGSO Journal of Australian Geology, v. 17(2); p. 63-75, 1997.
[23] C. A. Murphy, J. Brewster, "Target delineation using Full Tensor Gravity Gradiometry data", ASEG Extended Abstracts, vol. 1, pp. 1-3, 2007.
[24] J. D. Phillips, Processing and Interpretation of Aeromagnetic Data for the Santa Cruz Basin. Patahonia Mountains Area, South-Central Arizona, U.S. Geological Survey Open-File Report 02, 1998.
[25] R. W. Roest, J. Verhoef, M. Pilkigton, "Magnetic interpretation using the 3-D signal analytic", Geophysics, V. 57, pp. 116-125, 1992.
[26] R. J. Blakely, Potential Theory in Gravity and Magnetic Applications, Cambridge University Press, 441 p, 1995.
[27] J. B. C. Silva, V. C. F. Barbosa, "3D Euler deconvolution: Theoretical basis for automatically selecting good solutions", Geophysics, 68(6), 1962-1968, 2003.
[28] Y. Jeng, Y. L. Lee, C. Y. Chen, M. J. Lin, "Integrated signal enhancements in magnetic investigation in archaeology", Journal of Applied Geophysics, 53, pp. 31-48, 2003.
[29] R. J. Blakely, R. W. Simpson, "Approximating edges of source bodies from magnetic or gravity anomalies", Geophysics, 51(7), 1494-1498, 1986.

Author Profile

Alain Rodrigue Nzeuga received the B.S. in Physics and M.S. degrees in Geophysics from University of Yaounde I, Cameroon in 2006 and 2011, respectively. Currently, he is a Ph.D. student at the same university.